Journal of Intelligent and Robotic Systems **19:** 55–72, 1997.

Robotic Workspaces after a Free-Swinging Failure*

JAMES D. ENGLISH and ANTHONY A. MACIEJEWSKI
Purdue University, 1285 Electrical Engineering Building, West Lafayette, Indiana 47907-1285; e-mail: maciejew@ecn.purdue.edu

Abstract. A robotic manipulator can fail in many different ways, and its capabilities after a failure are a major concern, especially for manipulators used in hazardous and remote environments, where the cost of repair or replacement is high. This article presents a study of the workspaces of robotic arms after a free-swinging failure, defined as a hardware or software failure that prevents the application of actuator torque on a joint. Two analytical methods are discussed. The first is for planar arms only and is based on a positional inverse-kinematic algorithm that uses polynomial roots, guaranteeing that all solutions, and therefore the postfailure workspace, can be found. The second method has no such guarantee, but is applicable to general spatial manipulators. It is based on a differential technique for tracing the postfailure workspace boundary.

Key words: failure tolerance, free-swinging failure, hazardous environments, Hessian, joint torque, kinematic redundancy, postfailure workspace

1. Introduction

Robotic failure tolerance has received significant attention in the literature of late [1, 2, 3, 4]. Much of this work has addressed the type of robotic failure that causes a joint on a manipulator to become locked, either because the failure is intrinsically of the locking type or because brakes are applied to prevent erratic behavior. A principal concern when addressing the issue of failure tolerance is the capabilities of the manipulator after a failure, and a number of analyses of workspaces after a locked-joint failure have been made [5, 6, 7].

A robotic manipulator, however, can fail in many different ways, and it is important to also look at the capabilities of an arm after nonlocking failures. This article will focus on the free-swinging type of failure, defined as a hardware or software failure that prevents the application of actuator torque on a manipulator's joint. This type of failure could be caused, for example, by a ruptured seal on a hydraulic actuator or a loss of power on an electric motor. A free-swinging failure could also be partial, where limited actuator torque can be applied; this would occur, for example, when a weaker back-up actuator is used after a failure of the primary actuator.

After a free-swinging failure, the failed joint moves under the influence of external forces and gravity. This motion both fosters the potential for secondary damage and presents the possibility of expanded usefulness after a failure [8].

* This work was supported by Sandia National Laboratories under contract number AL-3011 and by a NASA graduate student research fellowship (grant number NGT9-2).

The issue of operating manipulators in anticipation of a free-swinging failure was addressed in [9]. It is the issue of usefulness after a failure as defined through the reachable hand poses that will be the focus of this article, and the emphasis will be on kinematically redundant arms. Kinematically redundant manipulators have been proposed for use in hazardous and remote environments due to their dexterity before a failure and ability to continue operation after a failure [10, 5, 7].

The postfailure workspace is defined here as the set of all hand poses reachable by the manipulator when stationary with zero actuator torque on the failed joint. The approach to analyzing it will be two fold. First, a method will be established for finding joint angles that give a desired hand pose without gravitational torque on a specific joint (the failed joint) for a three-link planar arm with mass distributions along the links. This will be used to analyze postfailure workspaces through exhaustive search. Second, a differential method will be presented for tracing the postfailure workspace boundary for a general spatial arm. In Section 4, the results of the two methods will be compared for the planar case, and the differential method will be used to find the postfailure workspaces for several arms where the first approach is not applicable.

2. The Workspace of a Three-Link, Planar Manipulator

In this section, the first of the two methods for analyzing postfailure workspaces will be given. It will be based on a zero-torque inverse-kinematics algorithm that guarantees discovery of all solutions for a class of planar arms with the task of end-point positioning. The approach will be as follows: First, a method will be given for solving the inverse kinematics for a specific case, that of zero gravitational torque on the base joint of a planar three-link manipulator with link masses at the ends of the links. Then a method will be given for mapping any joint failure for a wide class of three-link, planar manipulators into the specific case.

A. THE SPECIFIC CASE

Let the specific planar arm be defined as follows: The joint angle for link i is q_i, its link length is nonzero ℓ_i, its mass is m_i, and the center of mass of each link is located at the end of the link (i.e., centered at Denavit-Hartenberg (D-H) frame i). Define for each link i a pseudomass $\widehat{m}_i$. For the more general cases, $\widehat{m}_i$ will take on a different meaning and will allow the mapping from the more general into the specific, but here the pseudomass will equal the mass. That is,

$$\widehat{m}_i = m_i. \tag{1}$$

The geometric and inertial parameters of the specific arm are shown in Figure 1. The base frame will be defined such that the x-axis is perpendicular to the upward-pointing gravity vector $\mathbf{g}$, and $\mathbf{g} \cdot \hat{y} > 0$.

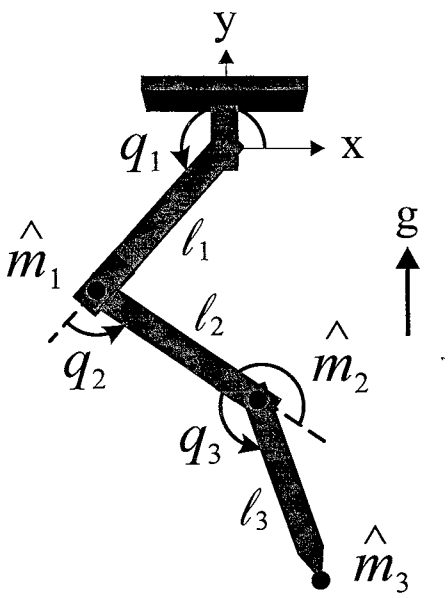

Figure 1. The specific manipulator. The link lengths are ℓ_i; the link masses are $\widehat{m}_i$; and the centers of mass coincide with the origins of the D-H frames (D-H frame n is defined, for convenience, to coincide with the tip). The q_i's are relative joint angles.

To simplify calculation of the zero-torque configurations, absolute angles ψ_i will be used; i.e.,

$$\psi_i = \psi_{i-1} + q_i; \quad \psi_0 = 0. \tag{2}$$

Also, the inward composite pseudomass will be used, defined through

$$\widehat{M}_i = \widehat{M}_{i+1} + \widehat{m}_i; \quad \widehat{M}_{n+1} = 0. \tag{3}$$

When there is no joint-one gravitational torque on the specific manipulator, the x-coordinate of the first-moment-of-inertia vector of the entire arm must vanish. This together with the end-effector-position constraint that the arm tip be located at (p_x, p_y) gives

$$\begin{bmatrix} c_1\ell_1 + c_2\ell_2 + c_3\ell_3 \\ s_1\ell_1 + s_2\ell_2 + s_3\ell_3 \\ \widehat{M}_1 c_1\ell_1 + \widehat{M}_2 c_2\ell_2 + \widehat{M}_3 c_3\ell_3 \end{bmatrix} = \begin{bmatrix} p_x \\ p_y \\ 0 \end{bmatrix}, \tag{4}$$

where $c_i = \cos(\psi_i)$ and $s_i = \sin(\psi_i)$. For stability, the y-coordinate of the first moment of inertia must be negative:

$$\widehat{M}_1 s_1\ell_1 + \widehat{M}_2 s_2\ell_2 + \widehat{M}_3 s_3\ell_3 < 0. \tag{5}$$

Using $\widehat{M}_3 = \widehat{m}_3$, the third entry of (4) gives the following equation in the absolute-angle cosines:

$$\widehat{m}_3 c_3 \ell_3 = -\widehat{M}_1 c_1 \ell_1 - \widehat{M}_2 c_2 \ell_2. \tag{6}$$

Then the first entry of (4) allows the elimination of c_3,

$$(\widehat{m}_2 \ell_2) c_2 = c_1 (\widehat{m}_3 \ell_1 - \widehat{M}_1 \ell_1) - \widehat{m}_3 p_x. \tag{7}$$

And the second entry of (4) allows elimination of c_2, giving

$$\pm\sqrt{A} \pm \sqrt{B} \pm \sqrt{C} = D, \tag{8}$$

where

$$A = \widehat{m}_2^2 \ell_3^2 - (c_1 \ell_1 \widehat{m}_1 + p_x(\widehat{m}_2 + \widehat{m}_3))^2, \tag{9}$$

$$B = \widehat{m}_2^2 \ell_1^2 (1 - c_1^2), \tag{10}$$

$$C = \widehat{m}_2^2 \ell_2^2 - (c_1 \ell_1 (\widehat{m}_1 + \widehat{m}_2) + p_x \widehat{m}_3)^2, \tag{11}$$

and

$$D = \widehat{m}_2 p_y. \tag{12}$$

Equations (6), (7), and (8) are necessary for (4) to be satisfied. Provided $\widehat{m}_2 \neq 0$ and $\widehat{m}_3 \neq 0$ they are restrictive in that they yield a finite number of solutions if only a finite number of solutions exist. Especially important, (8) is a necessary condition for c_1 alone. The square roots of (8) can be eliminated as follows:
Let

$$E = \tfrac{1}{2}(A - B - C - D^2) \tag{13}$$

and

$$F = E^2 + D^2 C - BC - D^2 B. \tag{14}$$

Then the following is a *necessary* condition for (8) to be satisfied:

$$F^2 - 4(B + E)^2 D^2 C = 0. \tag{15}$$

Using the values from (9)–(12), this gives a sixth-order polynomial equation in c_1. Provided the number of solutions is finite, this will give six, possibly nondistinct, values for c_1, which, as the roots of a polynomial, can always be found. Substituting these into Equations (7) and (6) gives six sets of cosines for joint angles one, two, and three. These typically correspond to 48 sets of angles (each cosine value apart from ± 1 gives two angle values). Since necessary conditions were used to find these angles, if a zero-torque solution exists, it must

be a member of this set. Spurious solutions can be eliminated by substitution into Equations (4) and (5).

B. THE GENERAL CASES

Now, let the geometry and inertia of a more general arm be defined as follows: The joint angle for link i is q_i; its link length is nonzero ℓ_i; its mass is m_i; and its center-of-mass lies at a distance of d_i in line along the link, i.e., at $(d_i - \ell_i, 0, 0)$ in D-H frame i. It is possible to use a polynomial-root-based method on planar manipulators with centers of mass that are not in line between D-H frames using an extension of the approach presented here.

B.1. No Torque on Joint One

Provided the link lengths ℓ_i are nonzero, the more general case with a failure of joint one can be mapped into the specific case by letting the pseudomasses of the links be given by

$$\widehat{m}_i = \frac{d_i m_i}{\ell_i} + \frac{\ell_{i+1} - d_{i+1}}{\ell_{i+1}} m_{i+1}; \quad m_{n+1} = 0. \tag{16}$$

A manipulator with pseudomasses $\widehat{m}_i$ at the D-H frame origins will have the same joint first moments of inertia and therefore will behave exactly like a manipulator with masses m_i located at d_i along each link for behavior not involving the second moment of inertia. Thus, after the mapping, (6), (7), and (8) can be used to find the solution sets for the more general arm provided $\widehat{m}_2 \neq 0$ and $\widehat{m}_3 \neq 0$, ensuring (6), (7), and (8) are restrictive. For the special cases of vanishing $\widehat{m}_2$ or $\widehat{m}_3$, (4) becomes simpler and can be solved using a different set of assumptions. Note the $\widehat{m}_i$'s may be negative – a negative mass value can be directly used in *Newton's Second Law of Motion* and its derivatives just as is a positive value.

B.2. No Torque on Joint Two

When there is no joint-two torque, the x-coordinate of the first-moment-of-inertia vector for links two and three must equal the x-coordinate of the second joint. This constraint can be mapped into (4) by first calculating $\widehat{m}_3$ and $\widehat{m}_2$ using (16) and then calculating $\widehat{m}_1$ as follows:

$$\widehat{m}_1 = -\widehat{m}_2 - \widehat{m}_3. \tag{17}$$

With this, (6), (7), and (8) can be used to find the solution sets for zero joint-two torque. Since there is no restriction on the value of $\widehat{m}_1$ in the specific solution, this will always work for $\widehat{m}_2, \widehat{m}_3 \neq 0$.

B.3. No Torque on Joint Three

When there is no joint-three torque, the x-coordinate of the first-moment-of-inertia vector for the third link must equal the x-coordinate of the third joint. This constraint can be mapped into (4) by first calculating $\widehat{m}_3$ using (16) and then calculating $\widehat{m}_2$ and $\widehat{m}_1$ as follows:

$$\widehat{m}_2 = -\widehat{m}_3 \tag{18}$$

and

$$\widehat{m}_1 = 0. \tag{19}$$

With this, (6), (7), and (8) can be used to find the solution sets for zero joint-three torque. This will always work for $\widehat{m}_3 \neq 0$. (Note this problem can be solved in closed form, using the fact that the last link must be vertical – the mapping here is for completeness.)

3. The General Workspace Boundary Problem

Let $\mathbf{q}$ be the column vector formed from the q_i's. Then for a general arm, the position and torque/force constraints for a stationary manipulator reaching hand pose $\mathbf{p}$ after a free-swinging failure of joint i (the general equivalent to (4)) are the following:

$$\mathbf{p} = \mathbf{f}(\mathbf{q}), \tag{20}$$

where $\mathbf{f}(\cdot)$ is the mapping from configuration to hand pose, and

$$\tau_i = 0, \tag{21}$$

where τ_i is the required actuator torque on rotational joint i or force on prismatic joint i. Since a stationary manipulator is assumed, the torque or force τ_i will typically equal g_i, the actuator torque/force due to gravity. For rotational joint i, gravitational g_i is given by

$$g_i = (\hat{z}_{i-1} \times \mathbf{s}^*_{i-1}) \cdot \mathbf{g}, \tag{22}$$

and for prismatic joint i by

$$g_i = M_i \hat{z}_{i-1} \cdot \mathbf{g}, \tag{23}$$

where $\hat{z}_\ell$ is the unit vector along joint $\ell+1$, the z-axis of the ℓth D-H coordinate frame; $\mathbf{s}^*_\ell$ is the first moment of inertia of the composite rigid body formed by links $\ell+1$ through n referred to the origin of D-H frame ℓ; $\mathbf{g}$ is the gravity vector in the upward direction; and M_i is the composite mass of the outboard links.

For rotational joints, the requirement for stability of the zero-gravitational-torque solution (when $\tau_i = g_i$) is that the composite center of mass of the links

outboard from the failed joint lie below – with respect to the gravitational field – the line coinciding with the axis of the failed joint. This is represented by the following:

$$(\mathbf{s}^*_{i-1} \times \hat{z}_{i-1}) \cdot (\hat{z}_{i-1} \times \mathbf{g}) > 0. \tag{24}$$

The composite first-moment-of-inertia vector $\mathbf{s}^*_i$ as expressed in the ith D-H frame can be calculated through the following two recursions:

$$M_i = m_i + M_{i+1}; \qquad M_n = m_n. \tag{25}$$

$$\mathbf{s}^*_i = {}^i\mathbf{R}_{i+1}(\mathbf{s}^*_{i+1} + \mathbf{s}_{i+1} + M_{i+1}\mathbf{p}_{i\to i+1}); \qquad \mathbf{s}^*_n = \mathbf{0}. \tag{26}$$

Here, ${}^i\mathbf{R}_{i+1}$ is the 3×3 rotation matrix representing D-H frame $i+1$ in frame i; $\mathbf{s}_\ell$ is the first-moment-of-inertia vector for link ℓ referred to and expressed in its own D-H frame; and $\mathbf{p}_{i\to\ell}$ is the vector from the origin of D-H frame i to the origin of frame ℓ, expressed in frame ℓ.

Solving the two nonlinear Equations (20) and (21) is a difficult problem for the general case, however, and it is useful to focus only on the postfailure workspace boundary. For this development, it will be assumed that there are no joint limits. Let the augmented Jacobian $\mathbf{J}_{A_i}$ be given by

$$\mathbf{J}_{A_i} = \begin{bmatrix} \mathbf{J} \\ \hline \nabla\tau_i^T \end{bmatrix}, \tag{27}$$

where $\mathbf{J}$ is the manipulator Jacobian. Then to be at a boundary configuration, provided τ_i is continuously differentiable, a necessary requirement in addition to (20) and (21) is

$$\text{rank}(\mathbf{J}_{A_i}) \leqslant m, \tag{28}$$

where m is the dimension of the task space (i.e., $\mathbf{J}$ is $m \times n$), for otherwise it would be possible to move in any direction while maintaining zero torque. Note also that if $\mathbf{p}$ is a boundary point of a region reachable with zero actuator torque through a given multiplicity of solutions, then (28) will be true for some zero-torque configuration reaching $\mathbf{p}$. This issue of solution multiplicity will be further addressed in Section 4.

The gradient of gravitational $\tau_i = g_i$ has entries $\partial g_i/\partial q_j$. For joint i rotational, using (22), the values of these entries are given by

$$\frac{\partial g_i}{\partial q_j} = \left(\left[\frac{\partial}{\partial q_j} \hat{z}_{i-1} \right] \times \mathbf{s}^*_{i-1} + \hat{z}_{i-1} \times \left[\frac{\partial}{\partial q_j} \mathbf{s}^*_{i-1} \right] \right) \cdot \mathbf{g}, \tag{29}$$

and for prismatic joint i, by

$$\frac{\partial g_i}{\partial q_j} = M_i \left(\frac{\partial}{\partial q_j} \hat{z}_{i-1} \cdot \mathbf{g} \right), \tag{30}$$

provided $\partial \hat{z}_{i-1}/\partial q_j$ and $\partial \mathbf{s}^*_{i-1}/\partial q_j$ are found with respect to the base frame and $\mathbf{g}$ is constant in the base frame.

When joint j is rotational, $\partial \hat{z}_i/\partial q_j$ and $\partial \mathbf{s}^*_i/\partial q_j$ can be found with respect to the base frame as follows:

$$\begin{aligned} \frac{\partial}{\partial q_j}\hat{z}_i &= \hat{z}_{j-1} \times \hat{z}_i, \quad j \leqslant i, \\ &= \mathbf{0}, \qquad\quad j > i, \end{aligned} \tag{31}$$

$$\begin{aligned} \frac{\partial}{\partial q_j}\mathbf{s}^*_i &= \hat{z}_{j-1} \times \mathbf{s}^*_i, \qquad j \leqslant i, \\ &= \hat{z}_{j-1} \times \mathbf{s}^*_{j-1}, \quad j > i, \end{aligned} \tag{32}$$

and when joint j is prismatic,

$$\frac{\partial}{\partial q_j}\hat{z}_i = \mathbf{0}, \tag{33}$$

$$\begin{aligned} \frac{\partial}{\partial q_j}\mathbf{s}^*_i &= \mathbf{0}, \qquad\quad j \leqslant i, \\ &= M_j \hat{z}_{j-1}, \quad j > i. \end{aligned} \tag{34}$$

Let a scalar boundary specifier $\aleph_i(\mathbf{q})$ be defined as a function of the joint variables that goes to zero if and only if $\mathbf{J}_{A_i}$ loses rank. For example, if $\mathbf{J}_{A_i}$ is square, $\aleph_i$ can be defined as

$$\aleph_i = \det(\mathbf{J}_{A_i}). \tag{35}$$

Then if τ_i continuously is differentiable, a particular configuration's hand pose is a postfailure workspace boundary point only if some configuration reaching it gives $\tau_i = 0$ and $\aleph_i = 0$. These conditions with (24) are sufficient for the point to be a stable postfailure workspace point when $\tau_i = g_i$. Note also that $\tau_i = \alpha$, any α, and $\aleph_i = 0$ are necessary conditions for a boundary point of the region reachable with $\tau_i = \alpha$.

If a manipulator is posed at a postfailure workspace boundary, then to trace the boundary, a necessary differential condition is a joint-rate vector perpendicular to both $\nabla\tau_i$ and $\nabla\aleph_i$. Such a trace may depart from the boundary (the conditions are only necessary), but will not depart from the postfailure workspace (for this, the conditions are sufficient). A discussion of the related issue of tracing algorithmic singularities is given in [11].

The gradient of $\aleph_i$ as defined through (35) can be found as follows:

$$\frac{\partial \aleph_i}{\partial q_k} = \text{trace}\left\{\frac{\partial \mathbf{J}_{A_i}}{\partial q_k}\text{adj}(\mathbf{J}_{A_i})\right\}, \tag{36}$$

where the partial derivative of $\mathbf{J}_{A_i}$ is the partial derivative of $\mathbf{J}$ concatenated with the partial derivative of $\nabla\tau_i$; i.e.,

$$\frac{\partial \mathbf{J}_{A_i}}{\partial q_k} = \begin{bmatrix} \frac{\partial}{\partial q_k}\mathbf{J} \\ \frac{\partial}{\partial q_k}\nabla\tau_i^T \end{bmatrix}. \tag{37}$$

Methods for calculating the partial derivative of the Jacobian are given in [12], and the partial derivative of gravitational $\nabla\tau_i = \nabla g_i$ can be found through the procedure below.

Entry j of $\partial\nabla g_i/\partial q_k$, equal to the entry (j,k) of the Hessian of g_i, is given by

$$\begin{aligned} &\frac{\partial^2 g_i}{\partial q_j \partial q_k} \\ &\quad = \left(\left[\frac{\partial^2}{\partial q_j \partial q_k} \hat{z}_{i-1} \right] \times \mathbf{s}^*_{i-1} + \hat{z}_{i-1} \times \left[\frac{\partial^2}{\partial q_j \partial q_k} \mathbf{s}^*_{i-1} \right] + \right. \\ &\qquad \left. + \left[\frac{\partial}{\partial q_j} \hat{z}_{i-1} \right] \times \left[\frac{\partial}{\partial q_k} \mathbf{s}^*_{i-1} \right] + \left[\frac{\partial}{\partial q_k} \hat{z}_{i-1} \right] \times \left[\frac{\partial}{\partial q_j} \mathbf{s}^*_{i-1} \right] \right) \cdot \mathbf{g} \end{aligned} \tag{38}$$

for a rotational joint, and

$$\frac{\partial^2 g_i}{\partial q_j \partial q_k} = M_i \left[\frac{\partial^2}{\partial q_j \partial q_k} \hat{z}_{i-1} \right] \cdot \mathbf{g} \tag{39}$$

for a prismatic joint, provided the partial derivatives are found with respect to the base frame and $\mathbf{g}$ is constant in the base frame.

The vectors $\partial^2 \mathbf{s}^*_i/\partial q_j \partial q_k$ and $\partial^2 \hat{z}_i/\partial q_j \partial q_k$ taken with respect to the base frame are given by the following for joints k and j rotational:

$$\begin{aligned} \frac{\partial^2}{\partial q_j \partial q_k} \hat{z}_i &= \hat{z}_{j-1} \times \frac{\partial}{\partial q_k} \hat{z}_i, \quad j < k \leqslant i, \\ &= \hat{z}_{k-1} \times \frac{\partial}{\partial q_j} \hat{z}_i, \quad k \leqslant j \leqslant i, \\ &= \mathbf{0}, \qquad\qquad \text{otherwise}, \end{aligned} \tag{40}$$

$$\begin{aligned} \frac{\partial^2}{\partial q_j \partial q_k} \mathbf{s}^*_i &= \hat{z}_{j-1} \times \frac{\partial}{\partial q_k} \mathbf{s}^*_i, \quad k > j, \\ &= \hat{z}_{k-1} \times \frac{\partial}{\partial q_j} \mathbf{s}^*_i, \quad k \leqslant j. \end{aligned} \tag{41}$$

When either (or both) of joints j and k are prismatic,

$$\frac{\partial^2}{\partial q_j \partial q_k} \hat{z}_i = \mathbf{0}. \tag{42}$$

For joint j rotational and k prismatic:

$$\frac{\partial^2}{\partial q_j \partial q_k}\mathbf{s}_i^* = \hat{z}_{j-1} \times \frac{\partial}{\partial q_k}\mathbf{s}_i^*, \quad k > j, \qquad = \mathbf{0}, \quad k \leqslant j. \tag{43}$$

For joint j prismatic and k rotational:

$$\frac{\partial^2}{\partial q_j \partial q_k}\mathbf{s}_i^* = \hat{z}_{k-1} \times \frac{\partial}{\partial q_j}\mathbf{s}_i^*, \quad k < j, \qquad = \mathbf{0}, \quad k \geqslant j. \tag{44}$$

And for joints j and k prismatic:

$$\frac{\partial^2}{\partial q_j \partial q_k}\mathbf{s}_i^* = \mathbf{0}. \tag{45}$$

Note that, unlike for the polynomial-root-based technique, the differential technique is not guaranteed to find the entire postfailure workspace to a prescribed level of discretization. As will be seen in examples to come, the postfailure workspace boundary may be composed of a number of disjoint sets satisfying the boundary condition. As is the typical case for finding zeros of complex nonlinear equations, there is no guarantee that an initial point in each of these sets can be found using a general nonlinear equation solving technique on (20) and (21). For the examples, this problem will be addressed by using a number of random initial conditions for the nonlinear equation solver and taking the union of the resulting traces.

4. Examples

In this section, an example planar manipulator will be used to compare the two analytical methods. The first method is guaranteed to correctly establish the postfailure workspace to the resolution of the exhaustive search and will be used to verify the second, differential method. Then the differential method will be used to find the postfailure workspace for a planar arm with offset link centers of mass and for a planar arm with springs on the joints. The first method as presented is not applicable to either of these cases. To further illustrate the generality of the second technique, the final example will be a four-link spatial manipulator.

A. PLANAR EXAMPLES

A.1. Using the Polynomial-Root-Based Method

The first example manipulator will have link lengths of unity, link masses of unity, and link centers of mass at the link centers (i.e., $d_i = 1/2, \forall i$). The gravity

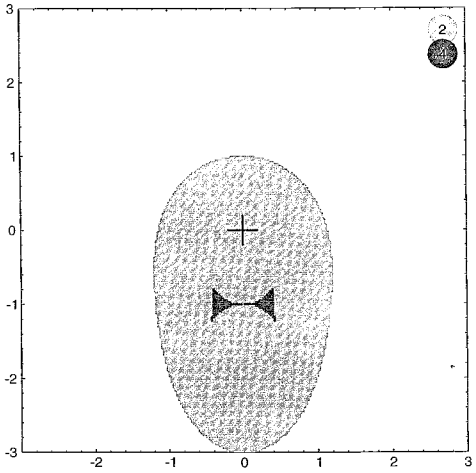

Figure 2. The numbers of solutions over the postfailure workspace of the example manipulator following a failure of joint one, as found using the zero-torque positional inverse kinematics. Any point in the light-gray region can be reached with two distinct configurations after a failure of the first joint, and each point in the dark-gray region can be reached with four.

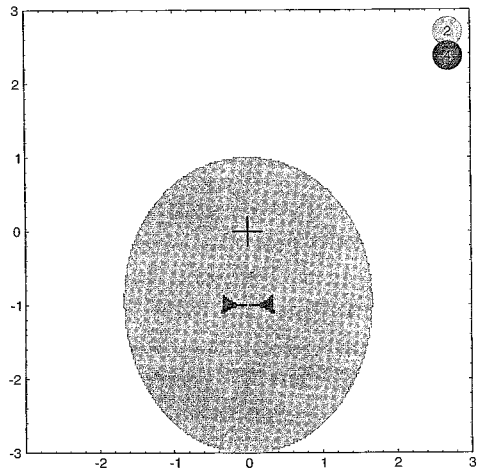

Figure 3. The numbers of solutions over the postfailure workspace of the example manipulator following a failure of joint two, as found using the zero-torque positional inverse kinematics. Any point in the light-gray region can be reached with two distinct configurations after a failure of the second joint, and each point in the dark-gray region can be reached with four.

vector will point in the y-direction of the base frame. To find the postfailure workspace of this arm using the first technique, a 160×160 grid was laid over the arm's workspace. Then, for each point on the grid, the zero-torque inverse-kinematic method was used to solve for all stable solutions. These were counted to get the value for that point on the grid.

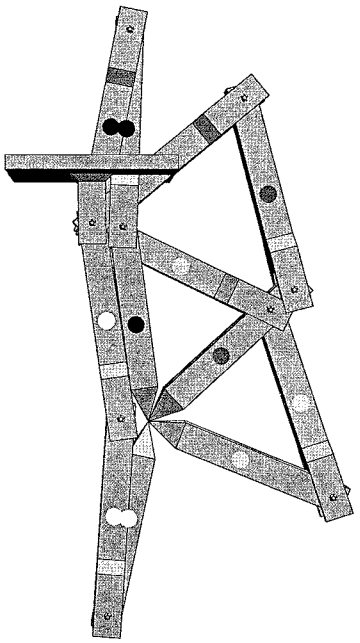

Figure 4. Four configurations reaching the point $(0.41, -1.01)$ with no torque on joint two. This point lies within the dark-gray region of Figure 3. Link centers of mass are shown by shaded disks. For each configuration, the center of mass of the composite body formed by links two and three lies below joint two, making each configuration stable.

The results of using this technique for a failure of joint one are shown in Figure 2, and the results for a failure of joint two are shown in Figure 3. The regions shown are for stable solutions, meaning the center of mass of the portion of the manipulator outboard from the failed joint lies below the failed joint (i.e., (5) applies). Any workspace point corresponding to a stable solution can be reached after a failure simply by moving the healthy joints to their required positions along an arbitrary path. Four configurations reaching a point within the dark gray region of Figure 3 are shown in Figure 4. For all the configurations, the composite center of mass of links two and three lies directly below the second joint.

A.2. Using the Differential Method

Provided ∇g_i and $\nabla \aleph_i$ are not linearly dependent, for a three-link manipulator a nonzero direction vector for tracing the gravitational postfailure-workspace boundary can be found using the vector cross product as follows:

$$\mathbf{d} = \nabla g_i \times \nabla \aleph_i. \tag{46}$$

This method was used to trace the boundary for the example planar arm of Section A.1 by first finding a solution to $g_i = 0$ and $\aleph_i = 0$ with a nonlinear equation

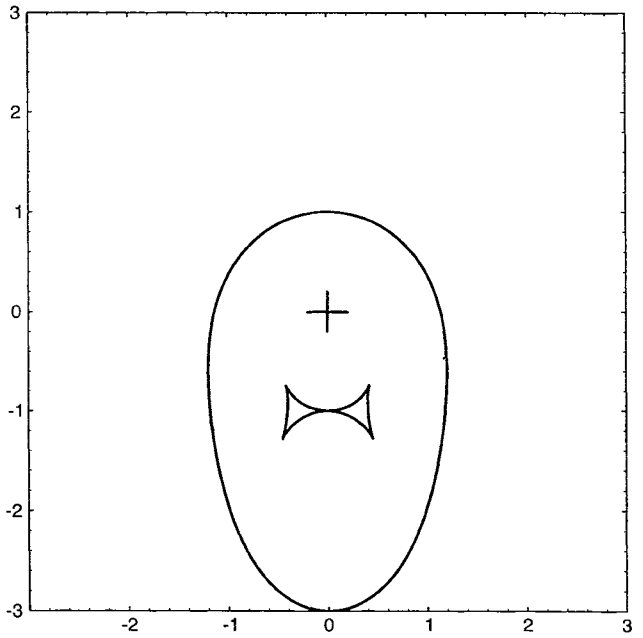

Figure 5. A trace of the stable postfailure workspace boundary of the example manipulator for a failure of joint one. These results agree with those found using the exhaustive-search method shown in Figure 2.

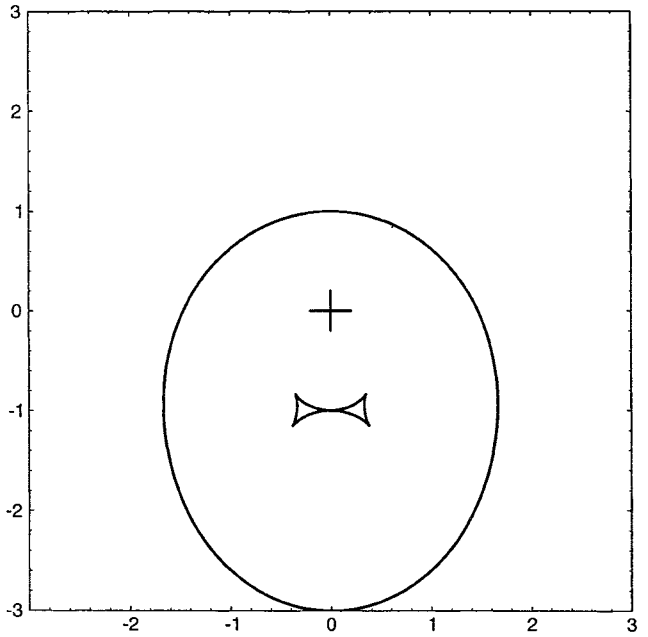

Figure 6. A trace of the stable postfailure workspace boundary of the example manipulator for a failure of joint two. These results agree with those found using the exhaustive-search method shown in Figure 3.

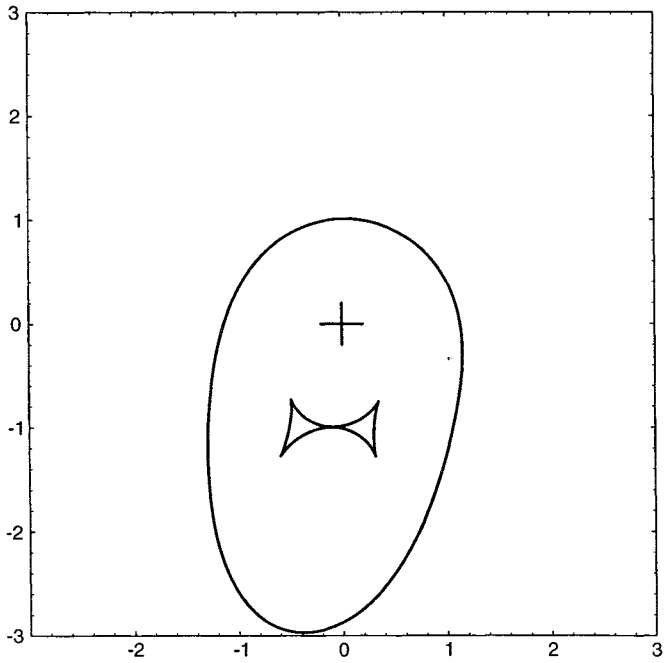

Figure 7. A trace of the stable postfailure workspace boundary for a failure of joint one, for the planar arm with the link centers of mass offset by $1/4$ link length from those of the previous example manipulator. These results are similar to those of the case with no offset shown in Figure 5.

solver, then taking discrete steps along the direction vector until returning to the starting configuration. To prevent drift due to the discrete steps, a feedback correction term for g_i and $\aleph_i$ was used. The boundary traces are shown in Figures 5 and 6. These results agree completely with those of the exhaustive-search method.

The tracing method is valid for a broader range of problems, however, and two additional applications are shown in Figures 7 and 8. Figure 7 gives the postfailure workspace boundary when the link centers of mass of the example arm are offset along the y-direction by $1/4$ link length. That is, each link's center of mass is located at $(-1/2, 1/4)$ in its own D-H frame, as compared to $(-1/2, 0)$ for the arm of Figure 5.

Figure 8 shows the postfailure workspace boundary for the example arm (no y-direction offset) after a joint-two failure with springs of stiffness numerically equal to $\|\mathbf{g}\|$ on the joints (for angles in radians); i.e., actuator torque is given by

$$\tau_i = g_i + \|\mathbf{g}\| q_i, \tag{47}$$

with g_i calculated using (22). The spring counters the force of gravity and enables the arm to reach farther away from the base, but not to reach near the base: the central tear-drop-shaped region is not reachable after a failure of the second joint. But even with this central void, the area of the postfailure workspace is much

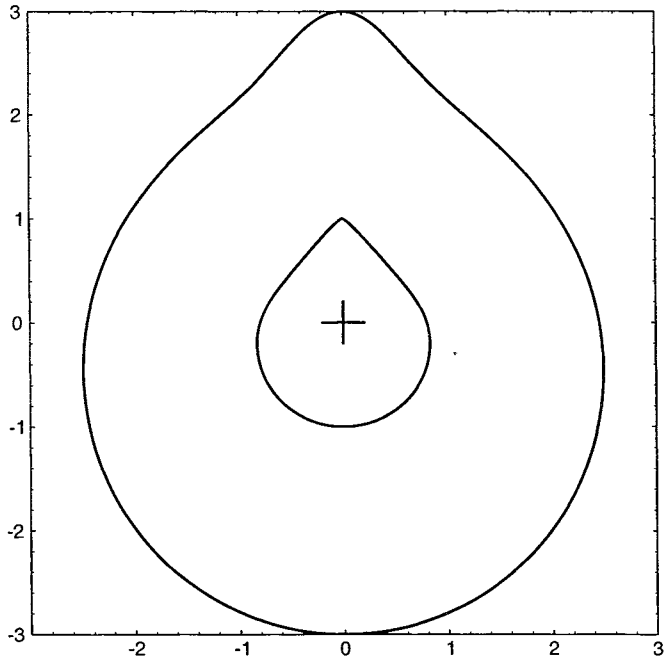

Figure 8. A trace of the postfailure workspace boundary for a failure of joint two, for the planar arm with a spring of stiffness numerically equal to $\|\mathbf{g}\|$ at joint two. These results vary considerably from those found for the case of no spring in Figure 6: the center region here has no solutions and the two-solution region is much larger.

larger in Figure 8 than in Figure 6, showing the benefit of using a spring. Any point lying between the two curves in Figure 8 is reachable after a failure, but the required positions of the healthy joints must be reached along a path that gives the required spring torque – i.e., it is path dependent.

B. A SPATIAL EXAMPLE

This section will study a spatial arm and will look at all zero-torque solutions, both stable and unstable. The example manipulator will be four link, with the following D-H parameters for all links i: $a_i = 1$, $d_i = 0$, $\alpha_i = \pi/2$, and $\theta_i = q_i$ (based on the labeling scheme of Paul [13]). Each link has unit mass, located at the link center $((-1/2, 0, 0)$ in its own D-H frame). The gravity vector points in the positive y-direction of the base frame, and the end-effector tip is located at the origin of the fourth D-H frame.

If a failure of joint i is the focus, then to trace the postfailure workspace boundary, a direction vector perpendicular to both ∇g_i and $\nabla \aleph_i$ is needed. Because there are four joints, the subspace of direction vectors at any boundary point is at least two dimensional. This allows a third constraint.

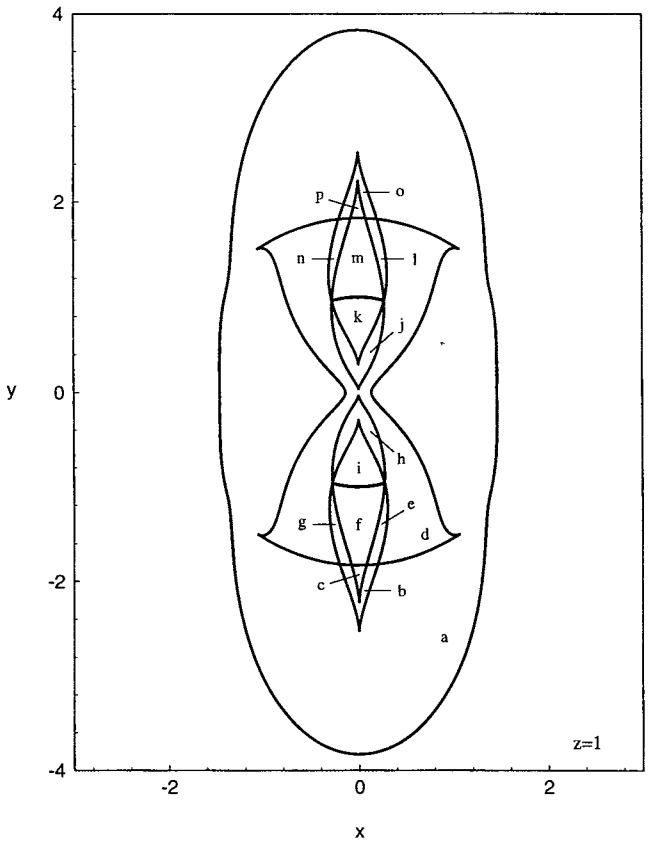

Figure 9. A trace in the $z = 1$ plane of the postfailure workspace boundary condition of the example spatial manipulator for a failure of joint one. There are 16 independent regions enclosed by boundary traces, labeled with the letters *a–p*. Points in region *a* have two zero-torque inverse-kinematic solutions; points in regions *b*, *d*, and *o* have four; points in regions *c*, *e*, *g*, *h*, *j*, *l*, *n*, and *p* have six; and points in regions *f*, *i*, *k*, and *m* have eight. These include all zero-torque solutions, both stable and unstable.

The constraint that will be used here is confinement of the trace to a plane. With this, the direction vector must induce tip motion perpendicular to the plane's normal. If $\mathbf{v}$ is the normal vector to the constraint plane, then a direction vector can be found as follows:

$$\mathbf{d} \in \mathcal{N}\left(\begin{bmatrix} (\nabla g_i)^T \\ (\nabla \aleph_i)^T \\ \mathbf{v}^T\mathbf{J} \end{bmatrix}\right), \tag{48}$$

where $\mathcal{N}(\cdot)$ denotes the null space.

The results of tracing the boundary condition for the example manipulator in the plane $z = 1$ are shown in Figure 9. There are 16 separate regions enclosed by the boundary-condition trace, each containing from two to eight solutions per

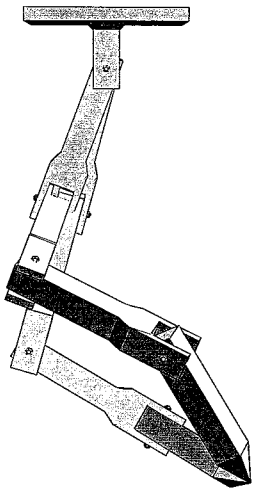

Figure 10. Two configurations of the example spatial manipulator with zero torque on the first joint reaching the point $(0.9, -2.6, 1.0)$. This point coincides with the location of the letter a in Figure 9.

point. All possible traces are shown (based on an extensive search), and hence the multiplicity of solutions cannot change within an enclosed region (where the region does not include the boundary points). Note, however, that the traces between regions f and i, and between k and m do not separate different solution multiplicities. The trace conditions are necessary for a multiplicity boundary, but not sufficient. Because both stable and unstable solutions were used in finding Figure 9, not all points are reachable by a slow-moving manipulator after an arbitrary joint-one failure. Two configurations reaching a point within the post-failure workspace with zero joint-one torque are shown in Figure 10. Both of these are stable solutions, satisfying (24).

5. Concluding Remarks

In this article, two methods were presented for analyzing robotic workspaces after a free-swinging failure. The first method involved solving the zero-torque inverse kinematics for a three-link planar manipulator. This was done by finding and solving a polynomial equation in the cosine of the first joint angle for a specific case and then mapping more general cases into the specific one using the concept of pseudomass. The second, differential, method involved defining a direction vector along which joint motion induced end-effector motion that followed the workspace boundary. This method was used to trace boundaries by discretizing motion along the direction vector and using feedback error correction

to prevent drift. As opposed to the polynomial-root-based method, the differential method could be used with any spatial or planar manipulator. The two methods agreed in examples where both were applicable, and the differential method was demonstrated in several examples for which the first method was not applicable.

References

1. Christensen, B., Drotning, W., and Thunborg, S.: Model-based, sensor-directed remediation of underground storage tanks, *J. Robotic Systems* **9**(2) (1992), 145–159.
2. Colbaugh, R. and Jamshidi, M.: Robot manipulator control for hazardous waste-handling applications, *J. Robotic Systems* **9**(2) (1992), 215–250.
3. Visinsky, M. L., Cavallaro, J. R., and Walker, I. D.: A dynamic fault tolerance framework for remote robots, *IEEE Trans. Robotics Automat.* **11**(4) (1995), 477–490.
4. Wu, E., Hwang, J., and Chladek, J.: Fault tolerant joint development for the space shuttle remote manipulator system: Analysis and experiment, in: *Proc. Fourth International Symposium on Robotics and Manufacturing (ISRAM '92)*, Sante Fe, NM, November 11–13, 1992, pp. 505–510.
5. Paredis, C. J. J., Au, W. K. F., and Khosla, P. K.: Kinematic design of fault tolerant manipulators, *Comp. Elec. Engnr.: An International Journal* **20**(3) (1994), 211–220.
6. Paredis, C. J. J. and Khosla, P. K.: Mapping tasks into fault tolerant manipulators, in: *Proc. 1994 IEEE Int. Conf. Robotics Automat.*, San Diego, CA, May 8–13, 1994, pp. 696–703.
7. Lewis, C. L. and Maciejewski, A. A.: Dexterity optimization of kinematically redundant manipulators in the presence of failures, *Comp. Elec. Engnr.: An International Journal* **20**(3) (1994), 273–288.
8. Arai, H. and Tachi, S.: Position control of a manipulator with passive joints using dynamic coupling, *IEEE Trans. Robotics Automat.* **7**(4) (1991), 528–534.
9. English, J. D. and Maciejewski, A. A.: Fault tolerance for kinematically redundant manipulators: Anticipating free-swinging joint failures, in: *Proc. 1996 IEEE Int. Conf. Robotics Automat.*, Minneapolis, MN, April 22–28, 1996.
10. Maciejewski, A. A.: Fault tolerant properties of kinematically redundant manipulators, in: *Proc. 1990 IEEE Int. Conf. Robotics Automat.*, Cincinnati, OH, May 13–18, 1990, pp. 638–642.
11. Klein, C. A., Chu-Jenq, C., and Ahmed, S.: A new formulation of the extended Jacobian method and its use in mapping algorithmic singularities for kinematically redundant manipulators, *IEEE Trans. Robotics Automat.* **11**(1) (1995), 50–55.
12. Lewis, C. L.: Fault tolerance for kinematically redundant manipulators, PhD thesis, Purdue University, 1994.
13. Paul, R. P.: *Robot Manipulators: Mathematics, Programming, and Control*, MIT Press, Cambridge, MA, 1981.